64th International Astronautical Congress, Beijing, China.

IAC-12-A6.2.7

ORBITAL DYNAMICS OF LIGHTWEIGHT FLEXIBLE DEBRIS

Mr. Sittiporn Channumsin
School of Engineering, University of Glasgow, United Kingdom
s.channumsin.1@research.gla.ac.uk

Dr. Matteo Ceriotti
School of Engineering, University of Glasgow, United Kingdom
matteo.ceriotti@glasgow.ac.uk

Dr. Carolin Früh
University of New Mexico, United States
cfrueh@unm.edu

Dr. Gianmarco Radice
School of Engineering, University of Glasgow, United Kingdom
Gianmarco.Radice@glasgow.ac.uk

An unexpected space debris population was recently identified as being very high area-to-mass ratio (HAMR) debris in geostationary orbit (GEO). Scientists hypothesised about their origins, consensus is that these objects are multi-layer insulation (MLI), separated from the spacecraft due to fragmentation events or delamination. These objects, like any other debris, pose a collision hazard for active satellites. Debris are usually considered rigid bodies; this assumption, however, is not fully justified for the MLI, as it lacks almost any structural strength. Large sheets of MLI are very flexible, and the change in geometry due to their flexibility can affect the effective area-to-mass ratio (AMR). This will cause varying effects due to external or internal forces and moments such as solar radiation pressure SRP, atmospheric drag, electromagnetic fields, or centrifugal and Coriolis forces. This, in turn, will affect the evolution of the orbital parameters, in a way that is difficult to predict. This paper introduces a simplified but effective model to represent the deformation of such debris, subject in particular to torques caused by solar radiation pressure and the Earth gravitational field, by means of Finite Element Method (FEM). This model adds a further set of dynamical equations, which accounts for the flexibility of the object, into the attitude and orbital equations; the resulting system is then numerically integrated to better evaluate the coupling between orbital and attitude dynamics. Due to a more precise estimation and prediction of the actual shape and orientation of the debris at any given time, than by simply assuming the case of a rigid body, the effects of the perturbations on the orbit can be computed more precisely, leading to improvements for the long-term prediction, over 150 days, of the orbital evolution. Results show that for debris in GEO the eccentricity change for flexible debris is different than for equivalent rigid bodies, and their attitude motions are unique.

I.INTRODUCTION

The Inter-Agency Agency Space Debris Coordination Committee (IADC) defines space debris as natural objects (e.g. comets, asteroids) or all artificial objects (e.g. rocket stages, inert satellites, adapters etc.). Artificial space debris can originate from many sources but collisions are undoubtedly a major issue. These debris orbiting with fast velocities are highly possible to threat the active satellites or generate new debris in space. A direct-ascent, kinetic-kill anti-satellite (ASAT) vehicle [1], for example, was successfully tested by destroying an inactive Chinese Feng Yun 1C (FY-1C) weather satellite on 11 January 2007. Xichang Space Centre and the US Space Surveillance Network (SSN) determined that over 900 pieces of hazardous debris were created by the impact. Two years later [2], a defunct Russian military satellite, Cosmos 2251, crashed into an active U.S. Iridium communications satellite. This collsion created two large debris clouds and SSN reported that 382 pieces of debris from Iridium33 and 893 pieces of debris from Cosmos 2251 were created from the collision.

The surveys of the European Space Agency (ESA) debris in GEO and nearby GEO with the ESA one metre ESA Space Debris Telescope (ESASDT) and Zimmerwald Laser, Astrometry Telescope (ZIMLAT), Schildknecht ([3], [4]) and the observations of the Astronomical Institute of the University of Bern (AIUB) 1-m telescope [5] aimed to understand the composition of the debris and light curves have been identified as the possible key to estimating both rotation and tumbling rates. Physical properties from observations by Jorgensen [6] and Mozurkewich [7] concluded that the

material exhibited High Area per Mass Ratio (HAMR) properties. One of many hypothesis as to their origin is delaminated Multi-Layer Insulation (MLI) debris. Generally, MLI, such as Kapton, Mylar, Teflon, Fluorinated Ethylene Propylene (FEP), Polyethylene Terephthalate (PET) and Tedlar or Polyvinyl fluoride film (PVF) is installed to reduce heat loss on board the spacecraft. From observations of the Hubble space telescope [8], a degradation of FEP surface of the MLI around the telescope was noticed. Further analysis of the size distributions and types of satellite breakup debris, were conducted by Murakami and Sen ([9], [10]). The results show that the pieces of satellite are not only metal panels and electronic circuits but also MLI, and Carbon Fibre Reinforced Plastics (CFRP).

The perturbations that affect the orbital motion of these objects are solar radiation pressure, the Earth's shadowing effects, and luni-solar third body attraction. Liou [11] studied the orbital dynamics of HAMR objects in GEO with two numerical solvers: SPCM and PROP3D while Früh [12] investigated reflection properties and the light curves that were measured from the variation of the brightness of the object under perturbations in GEO. The coefficient of reflectivity, C_r, of the surface was studied by Anselmo, [13] to study debris's orbit with A/M and Kelecy estimated the orbit of a known HAMR debris(a flat plate cooler cover from MSG-2) and the results are compared to actual observational data of a known HAMR debris. The approach is generally valide when the source of debris is available data.

Valk [14] applied semi-analytical theory and perturbations for investigation of the Earth's shadowing effects to HAMR in GEO. Mean Exponential Growth factor of nearby orbits (MEGNO) propagator was applied by Valk to propagate the dynamics of HAMR in GEO [15]. One of Anselmo's study [13], investigated breakup fragments from optical observation in GEO regime under perturbations in long-term over century. The results show that the high area-to-mass ratio(A/M) affects the oscillations of eccentricity, inclination including a lifetime of debris.

Fegel, [16] simulated MLI debris with the Meteoroid And Space Debris Terrestrial Environment Reference Model (MASTER) 2009 and validated it by comparison with observational data from ESA's space debris telescope. Mozurkewich [7] assumed three different typologies: synthetic pinwheel, asymmetric pinwheel and flake pinwheel and add the flexibility of MLI debris that will affect the light-curve of them. The study shows that the angular momentum depends on A/M ratio, irregularity of shape reflectivity internal friction and perturbations for light-curve interpretation. Früh ([17] ,[18])continued to investigate MLI over short time frames under the Earth's gravitation, third body from the Sun, SRP perturbation and the Earth's shadow The results show that the different initial conditions of attitude motion results in significant changes in term of orbit element and the shape of the MLI debris influences unique attitude motion and the volume entity of the disturbances. Thus, it is believed that the deformation is one of the main contributing factors to increase the accuracy of orbit determination of flexible debris.

In this paper, we will use a Finite Element Method (FEM) to model the deformation of flexible debris considering only in one plane for this preliminary study and propagate the coupling of orbit and attitude dynamics over orbits in the GEO region in 3D. We will consider two configurations: flat sheet and folded flat plate and try to understand their evolution subject to environmental perturbations due to Earth gravitation, third body gravitation from the Sun and Moon and the solar radiation pressure.

II. ORBITAL AND ATTITUDE DYNAMICS

II.I Orbital Dynamics

When modeling the force environment, the perturbations acting on objects are typically modeled by applying a gravity field from the Earth, third body gravity forces due to the Sun and Moon and may include tides, atmospheric drag, solar radiation pressure and other effects as deemed necessary.

In this paper, the perturbative forces that will be considered are: Earth gravitational field, presence of Sun and Moon [19] and SRP as described in Eq. [1].

$$\ddot{\vec{x}} = -GM_{\oplus}\nabla V(\vec{x}) - G\sum_{k=1,2} M_k \left[\frac{\vec{x}-\vec{x}_k}{\left|\vec{x}-\vec{x}_k\right|^3} + \frac{\vec{x}_k}{\vec{x}_k^3} \right] + \vec{a}_{SRP} \quad [1]$$

Where G is the gravitational constant, $M_{\oplus}$ is the Earth's mass, $\vec{x}$ is the geocentric position and velocity vector of the object w.r.t. the Earth and V is the potential gravitation, the third body gravitational perturbations of the Sun and Moon (k = 1, 2) respectively and SRP acceleration The SRP force [18] depends on the area and its orientation exposed to the radiation coming from the Sun:

$$\vec{F}_{rad,i} = A_i \frac{E}{C}\frac{AU^2}{\left|\vec{x}_i-\vec{x}_{\oplus}\right|^2}\vec{S}\vec{N}_i\left[(1-C_{s,i})\vec{S}+2(C_s \bullet \vec{S}\vec{N}_i+\frac{1}{3}C_d)\vec{N}_i\right] \quad [2]$$

thus we can calculate the SRP acceleration from Eq. [2] as following:

$$\vec{a}_i = \frac{\sum_{i=1}^{n}\vec{F}_{rad,i}}{m} \quad [3]$$

In these formulas, A is the cross sectional area reflecting SRP, m is the mass of the object, and C_d and C_s are the coefficients of diffuse and specular reflectivity, respectively [19]. The surface normal unit

vector, $\vec{n}$, and the solar incidence vector, $\vec{s}$, are required to specify the orientation of the satellite. The summation adds the *n* flat plate surfaces of the satellite model, while the i[th] subscript defines the area of each plate, angle and coefficients of each macro model plate. *E* is the solar constant, *C* is velocity of light, AU is the astronomical unit, is the position vector to the centre of pressure of the i[th] surface and $\vec{x}_{\oplus}$ is the geocentric position of the Sun.

II.II Attitude Dynamics

The attitude is studied by using Euler equation:

$$\dot{H} = \frac{d(I\mu)}{dt} = \sum^{2} - \vec{\mu} \times (I\vec{\mu}) \qquad [4]$$

Where $\dot{H}$, is derivative of the angular momentum, is the total external torque about the centre of mass, $\sum^{2}$ is the total angular momentum of system acting on the body, *I* is moment of inertia of objects and $\vec{\mu}$ is angular velocity.

For the kinematic equations of the Euler parameters ,they are represented in the time derivative of its relative orientation of debris from the angular rate in body frame. They are useful to propagate the attitude of satellite. We, however, apply in term of the time derivative of the unit quaternion in a body-fixed reference frame to our model in Eq. [5] but the results are shown via Euler angles, which are more intuitive to understand and visualise.

$$\frac{d\vec{q}}{dt} = \frac{1}{2}\Omega \bullet \vec{q} \qquad [5]$$

and

$$\Omega = \begin{bmatrix} 0 & \mu_3 & -\mu_2 & \mu_1 \\ -\mu_3 & 0 & \mu_1 & \mu_2 \\ \mu_2 & -\mu_1 & 0 & \mu_3 \\ -\mu_1 & -\mu_2 & -\mu_3 & 0 \end{bmatrix} \qquad [6]$$

The direct solar radiation torque is represented as follows [20]:

$$^{2}_{rad} = -\sum_{i=1}^{n} (^{\circ}_{CoM} + ^{\circ}_{CoP}) \times (T \bullet \vec{F}_{rad}) \qquad [7]$$

where $^{\circ}_{CoM}$ is the centre of mass of the object in the body frame reference, $^{\circ}_{CoP}$ is the center of pressure, *T* is the transformation matrix from the reference frame to the body frame and $\vec{F}_{rad}$ is solar radiation force. The gravitational torque [21] is derived by the gravitational force acting on the debris from:

$$^{2}_{grav} = \frac{3GM_{\oplus}}{R^3}(\vec{R}x I\vec{R}) \qquad [8]$$

where $\vec{R}$ is the transformation from the unit vector w.r.t. the Earth to body frame.

II.III Finite element analysis

Bernoulli-Euler theory [22] is used here to investigate the deformation of debris. Fig 1 represents a beam with two nodes. The vector of global displacement, *E* is Young's Modulus, *A* is cross-section and *I* is the second moment of inertia and each node has three global degrees of freedom, two displacement in *x*, *y* axis and one rotation.

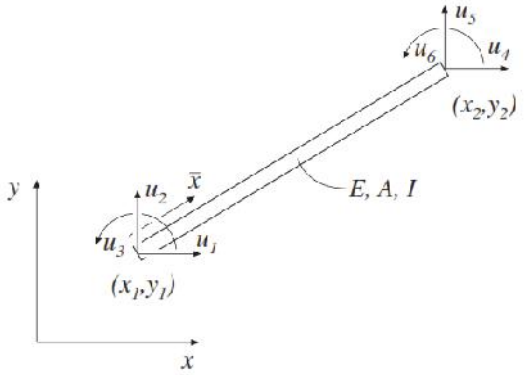

Fig 1 Bernoulli beam element with 2 nodes.

The vector of displacement is given by:

$$U = \begin{bmatrix} U_1 & U_2 & U_3 & U_4 & U_5 & U_6 \end{bmatrix}^T \qquad [9]$$

Where U_1, U_2 and U_3 are x and y displacement and rotation of the 1[st] node respectively, U_4, U_5 and U_6 are x and y displacement and rotation of the 2[nd] node respectively. In this study, the debris will have nine degrees of freedom space. To simplify only the linear dynamics will be considered:

$$M\ddot{U} + C\dot{U} + KU = F \qquad [10]$$

where U, $\dot{U}$ and $\ddot{U}$ are the vectors of generalized displacement, velocity and acceleration respectively :

$$U = \begin{bmatrix} U_1 \\ U_2 \\ U_3 \\ U_4 \\ U_5 \\ U_6 \end{bmatrix} \quad \dot{U} = \begin{bmatrix} \dot{U}_1 \\ \dot{U}_2 \\ \dot{U}_3 \\ \dot{U}_4 \\ \dot{U}_5 \\ \dot{U}_6 \end{bmatrix} \quad \ddot{U} = \begin{bmatrix} \ddot{U}_1 \\ \ddot{U}_2 \\ \ddot{U}_3 \\ \ddot{U}_4 \\ \ddot{U}_5 \\ \ddot{U}_6 \end{bmatrix} \qquad [11]$$

Also, *F* is the force matrix which consists of forces along the x and y axis and *M*:

$$F = \begin{bmatrix} F_{x1} \\ F_{y1} \\ M_1 \\ F_{x2} \\ F_{y2} \\ M_2 \end{bmatrix} \quad [12]$$

M is the mass matrix standard of Bernoulli-Euler Beam element in local coordinates:

$$\overline{M} = \frac{mL}{420}\begin{bmatrix} 140 & 0 & 0 & 70 & 0 & 0 \\ 0 & 156 & 22L & 0 & 54 & -13L \\ 0 & 22L & 4L^2 & 0 & 13L & -3L^2 \\ 70 & 0 & 0 & 140 & 0 & 0 \\ 0 & 54 & 13L & 0 & 156 & -22L \\ 0 & -13L & -3L^2 & 0 & -22L & 4L^2 \end{bmatrix} \quad [13]$$

Where m is mass of an element and L is length of an element

And K is the stiffness matrix standard of Bernoulli-Euler Beam element in local coordinates:

$$\overline{K} = \begin{bmatrix} \frac{EA}{L} & 0 & 0 & -\frac{EA}{L} & 0 & 0 \\ 0 & \frac{12EI}{L^3} & \frac{6EI}{L^2} & 0 & -\frac{12EI}{L^3} & \frac{6EI}{L^2} \\ 0 & \frac{6EI}{L^3} & \frac{4EI}{L} & 0 & -\frac{6EI}{L^2} & \frac{2EI}{L} \\ -\frac{EA}{L} & 0 & 0 & \frac{EA}{L} & 0 & 0 \\ 0 & -\frac{12EI}{L^3} & -\frac{6EI}{L^2} & 0 & \frac{12EI}{L^3} & -\frac{6EI}{L^2} \\ 0 & \frac{6EI}{L^2} & \frac{2EI}{L} & 0 & -\frac{6EI}{L^2} & \frac{4EI}{L} \end{bmatrix} \quad [14]$$

II.IV Coordinate transformation

We can transform from a body frame of reference to an inertial frame of reference by using a transformation matrix:

$$T = \begin{bmatrix} c & s & 0 & 0 & 0 & 0 \\ -s & c & 0 & 0 & 0 & 0 \\ 0 & 0 & 1 & 0 & 0 & 0 \\ 0 & 0 & 0 & c & s & 0 \\ 0 & 0 & 0 & -s & c & 0 \\ 0 & 0 & 0 & 0 & 0 & 1 \end{bmatrix} \quad [15]$$

where

$$c = \cos^{-} = \frac{x_2 - x_1}{L} \text{ and } s = \sin^{-} = \frac{y_2 - y_1}{L} \quad [16]$$

Thus, the stiffness matrix and mass matrix in inertial coordinates are defined as:

$$K = T^T \overline{K} T \text{ and } M = T^T \overline{M} T \quad [17]$$

Finally, the most common approach is to define the damping matrix C, through Rayleigh damping [23], which assumes a proportionality to the mass $\overline{M}$ and stiffness $\overline{K}$. This equation is given by:

$$C = \sim \overline{M} + \quad \overline{K} \quad [18]$$

Where ~ and are proportional damping coefficients

III. SIMULATON ANALYSIS

The aim of this analysis is to compare the orbit propagation of a debris considered as rigid body and the propagation of a debris including its deformation. According to most observations, MLI debris is found in the GEO region. We will assume the initial orbital parameters are defined as:

Table 1 The initial six Keplerian's elements

Keplerian's elements	
a (km)	41,254
e	0.0001
i (deg)	30
Ω (deg)	45
ω (deg)	14
M (deg)	210

The initial position is set as outlined in while the initial attitude is defined with all Euler angles and rates set to zero degrees.

Reflection and material properties of multi-layer insulations are based on [24]. The basic structure of MLI is composed of a single sheet of MLI, made of Polyethylene terephthalate (PET), thickness of 6 μm, and the aluminium coating is 1000 Á thick on both sides. This investigation assumes to be one layer of PET to simplify the model.

Two different forms of MLI are considered for the simulations: a flat sheet and a flat sheet which is folded along the middle at an angle of 90 degrees as in Fig. 2(a)**,** dashed line. The dimensions of both configurations are: 1 meter of width and length, thickness of 6 μm. [25, 26]. The properties of the material are shown in and this yields an area per mass ratio of: 119.90 m^2/kg.

Table 2 Properties of PET material

Type material	Mass Density [kg/m3]	Young's Modulus [N/m2]	Poisson 's ratio	*Cs*, *Cd*, *Ca*
PET	1,390	$3.10x10^9$	0.38	0.6 0.26 0.14

For long term analysis the Sun and Moon vectors with respect to the Earth are significant factors to consider for the orbital evolution and attitude behaviour of the debris. They are calculated by using the number of Julian centuries [19]to find the ecliptic longitude, obliquity of ecliptic before compute the Earth-Sun vector in term of coordination. The Earth-Moon vector is required the ecliptic latitude, longitude including parallax before computing the vector. Moreover, the Earth eclipse is considered and modelled to be a perfectly cylinder shadow.

III.I Deformation results validation

To validate the FEM code for deformation of flexible material, we define that each feature consisting 2 elements, which have 3 nodes, red points, and apply force, 8.011e-7 N, at the 1st node, blue direction, following Fig 2(a) and we define the boundary condition of degrees of freedom ,nine degrees. We integrate the differential equations of motion with ODE45 function in MATLAB to study the deformation for 3 seconds. The results are shown in Fig 2 and Fig 3.

In Fig 2(a), the 1st node displacement moves to the right side while the 3rd node move downwards. The 1st node of the flat plate in Fig 3(a) moves down and results pulls with it the 2nd and 3nd nodes due to tension forces. These results are used to validate the simple model of the natural displacements of low weight and thin material. Due to the deformation in Fig 2(b) and Fig 3(b), the centre of mass moves from its initial position. As a result, it affects the attitude motion of the debris as shown in the next section.

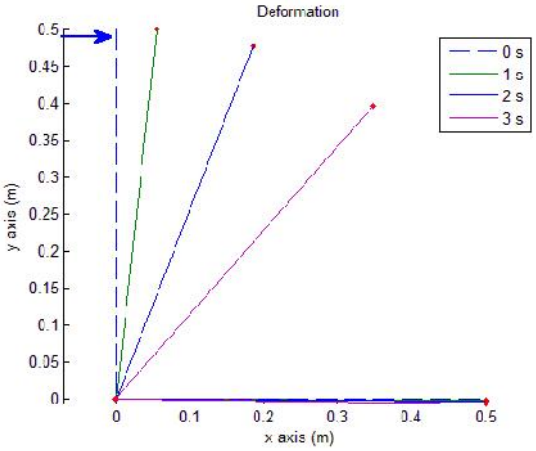

a)

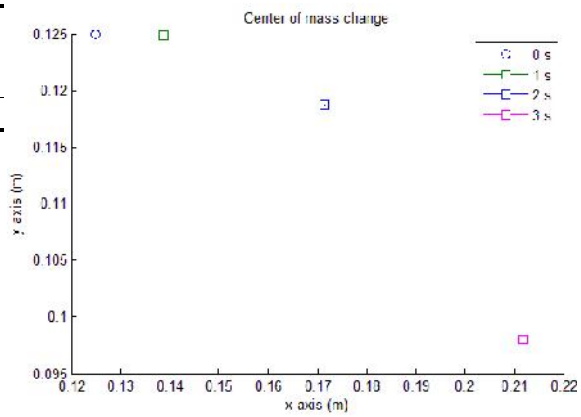

b)

Fig 2 a) Deformation of folded flat plate at 0, 1, 2 and 3 s by force 8.011e-7 N in the first node in right direction b) The change of center of mass of folded flat plate at 0, 1, 2 and 3 s

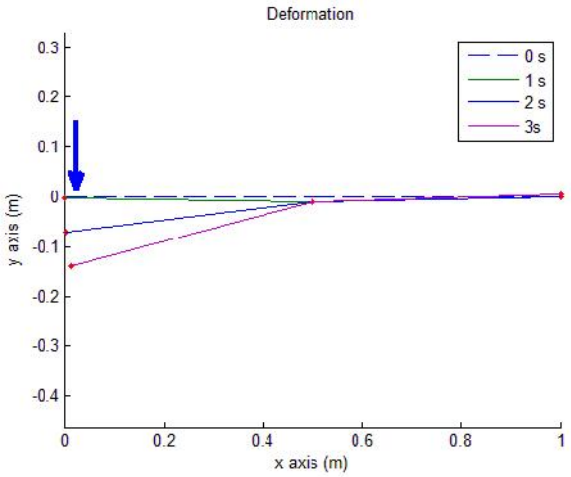

a)

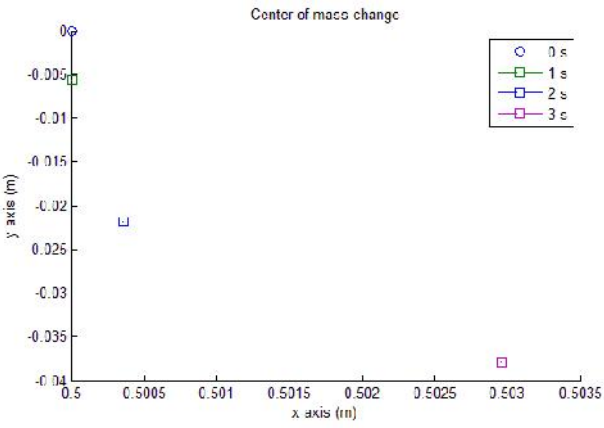

b)

Fig 3 a) Deformation of flat plate in 0.2, 0.4 and 0.6 s due to a force of 8.011e-7N in the first node in -y direction b) The change of center of mass of flat plate

III. II Numerical Integration methods

The numerical integration to solve the propagation of the second order differential equations of orbital and attitude equations used here is the Runge-Kutta method in MATLAB, ODE45 by converting the 2nd order equations to an equivalent system of 1st order equations before coupling with orbit, attitude and deformation equations.

IV. RESULTS

The Earth gravitation, third body from the Sun and Moon and SRP radiation pressure have been applied to four different configurations characteristics, rigid flat sheet, flexible flat sheet, rigid folded plate and flexible folded plate. The evolution of eccentricity and inclination over 3 days are shown in Fig 4 and Fig 5 while a long term propagation for over 150 days are shown in Fig 6and Fig 7. In Fig 4(a), eccentricity of rigid body grows up consistently while those of flexible body are different that fluctuate in same peak of range and inclination and it is very obvious in Fig 4(b) to see inconsistency of flexible debris of both initial geometry of flat plate and folded plate. In Fig 5(a), they have similar trend to increase but the flexible debris are below that of the rigid body in Fig 5(b). To monitor in the long period, the mean eccentricity of the orbit of the rigid body increases (Fig 6) while in the case of flexible debris do not rise significantly. The mean inclination for the rigid debris in Fig 7 increases while for flexible debris it oscillates around a mean value. The reason of this can be found in the change of the cross-sectional area due to the deformation of the sheet, effectively changing exposed area to solar radiation pressure and sun angles.

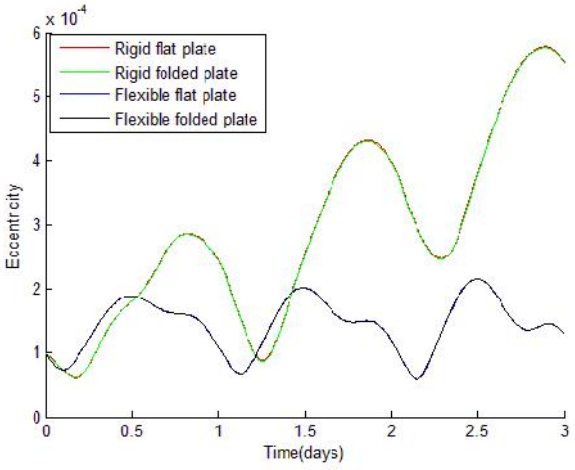

a)

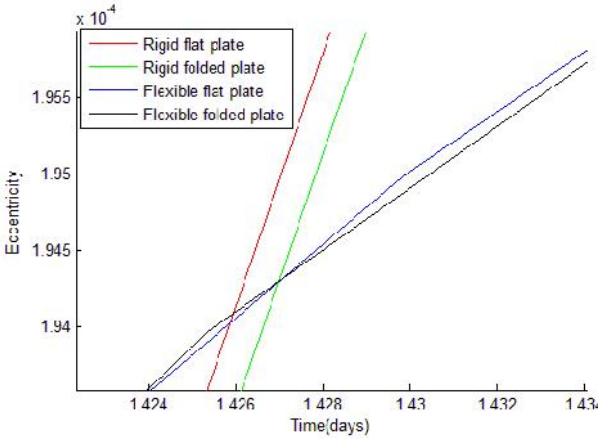

b)

Fig 4a) Eccentricity of flat plate and folded up flat plate in both rigid and flexible cases b) Magnify eccentricity period of 1.42 – 1.44 days

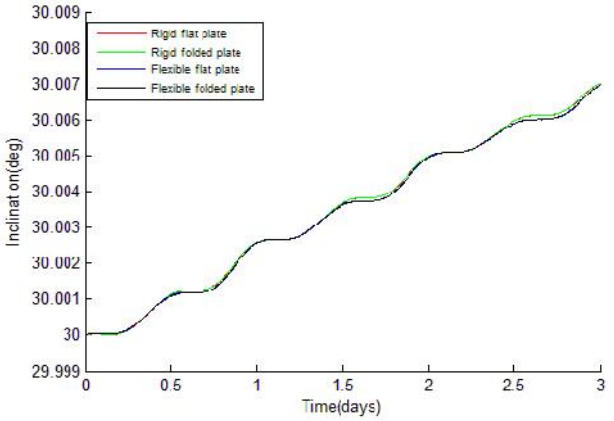

a)

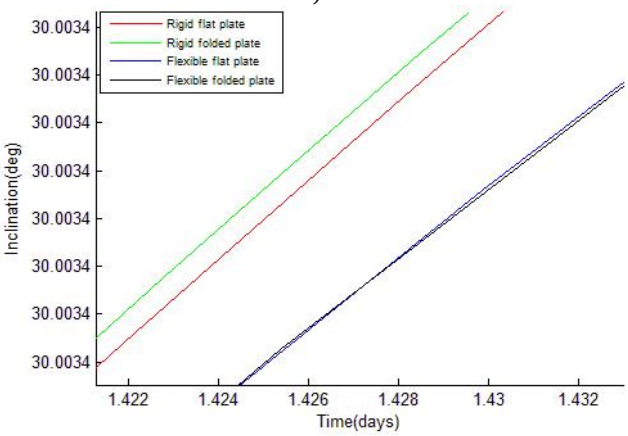

b)

Fig 5 a) Inclination of flat plate and folded up flat plate in both rigid and flexible cases b) Magnify inclination period of 1.42-1.43 days

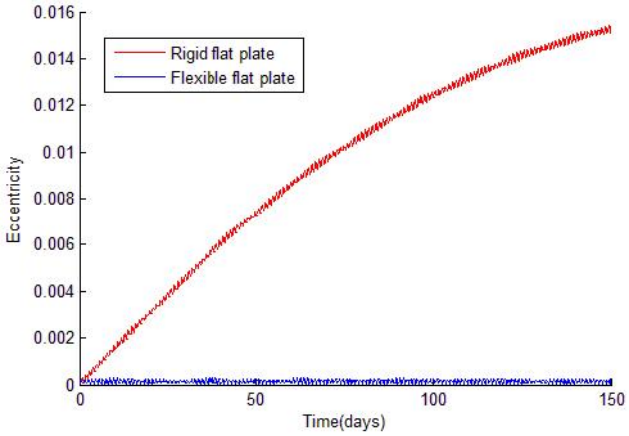

a)

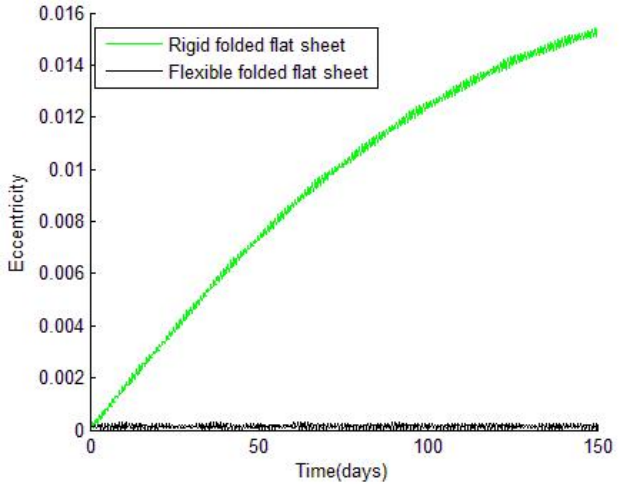

b)

Fig 6 a) Eccentricity of flat plate in both rigid and flexible cases in 150 days b) Eccentricity of folded flat plate in both rigid and flexible cases in 150 days

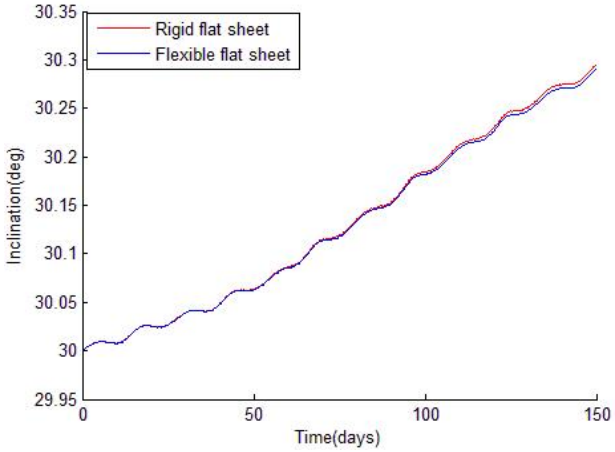

a)

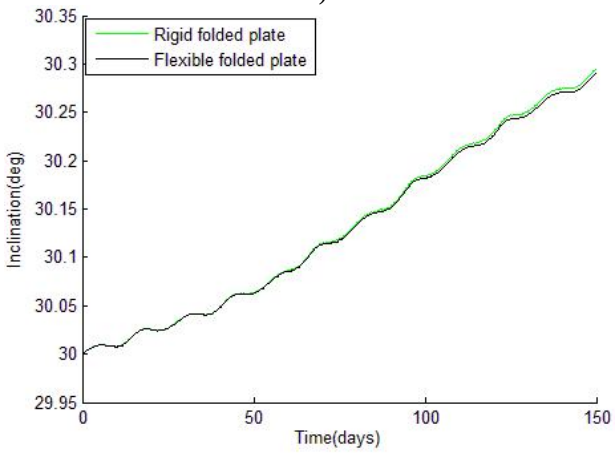

b)

Fig 7 a) Inclination of flat plate in both rigid and flexible cases in 150 days b) Inclination of folded flat plate in both rigid and flexible debris in 150 days

In Fig 8 and Fig 9, the attitude of the flexible debris in both configurations appears to rotate significantly slower than for the rigid debris for which the flat configuration presents the fastest displacements. As a result of deformation, the centre of mass and moments of inertia are always changing, leading to continuously varying effects from SRP and gravitational torques. After propagating over 150 days in

Fig 10, Fig 11, Fig 12 and Fig 13, the flexible debris, shows periods of small changes alternating with periods of high fluctuations. This effect does not occur for the rigid debris which exhibits a more uniform behavior in time.

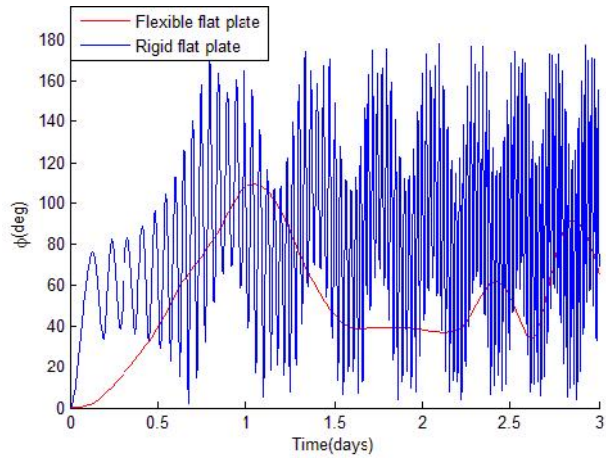

a)

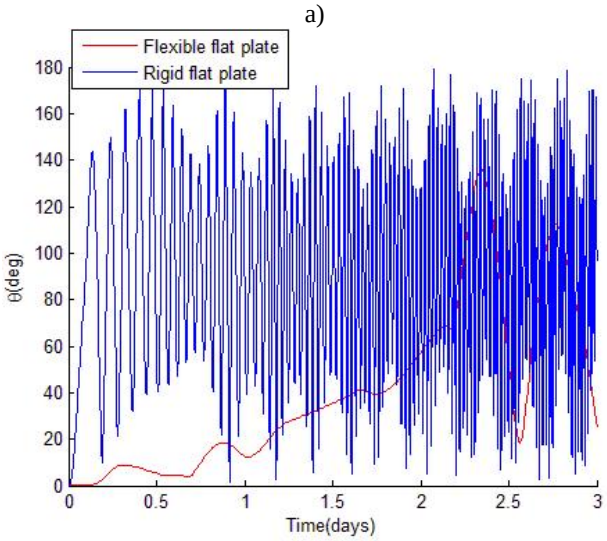

b)

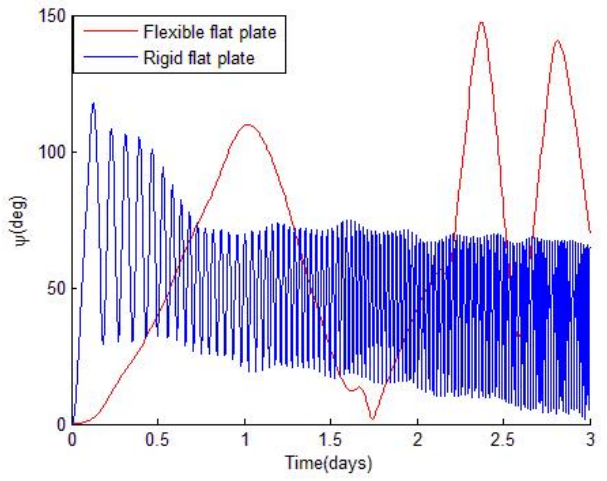

c)

Fig 8 Euler angles of flat plate in case of rigid body and flexible body in 3 days

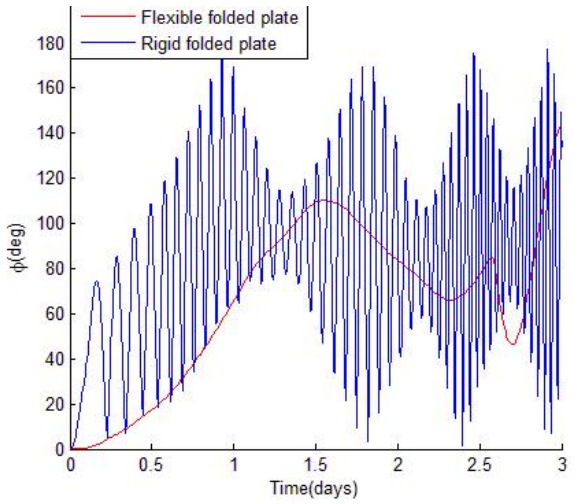

a)

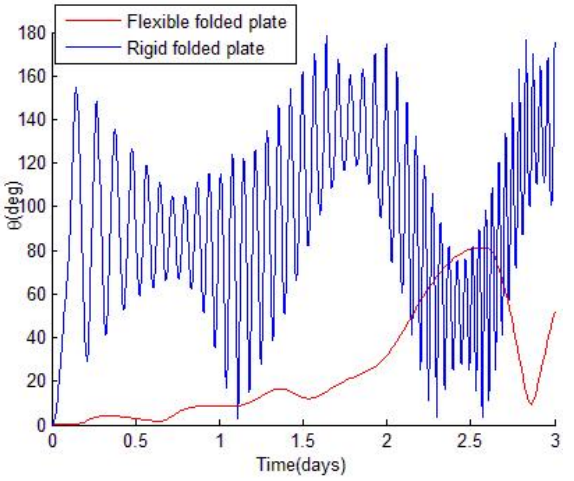

b)

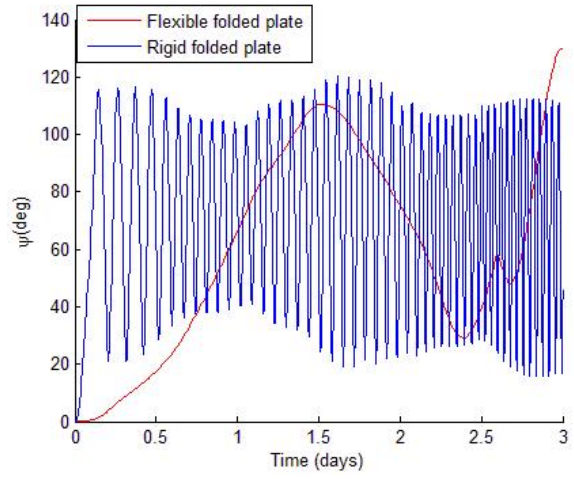

c)

Fig 9 Euler angles of folded flat sheet in case of rigid body and flexible body in 3 days

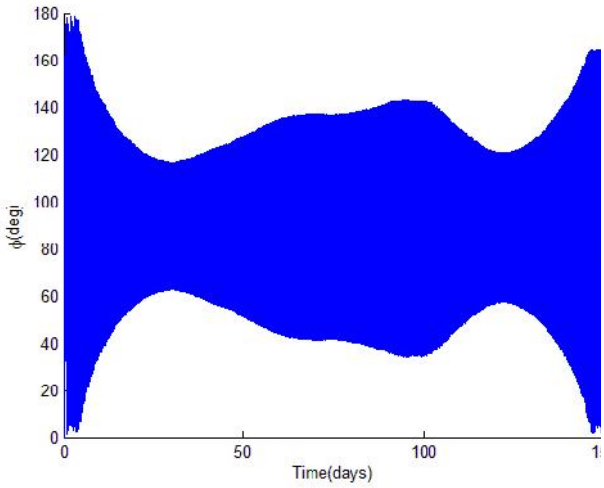

a)

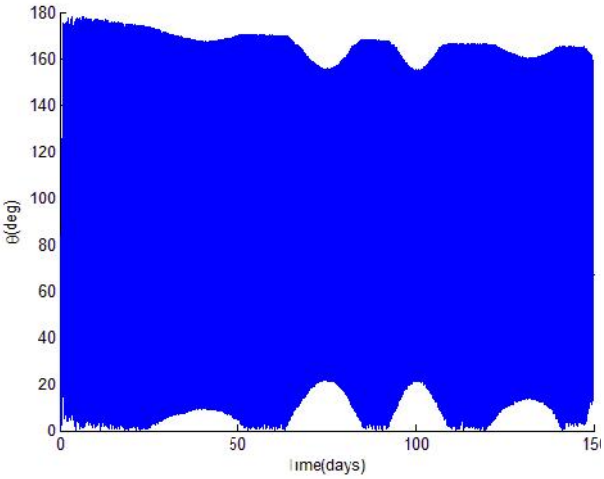

b)

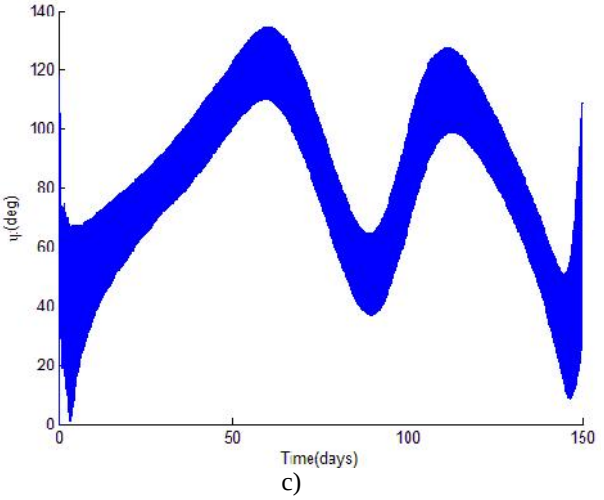

c)

Fig 10 Euler angles of rigid flat plate in 150 days

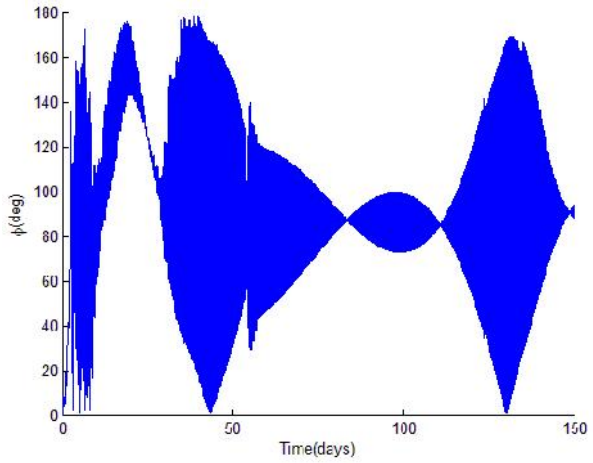

a)

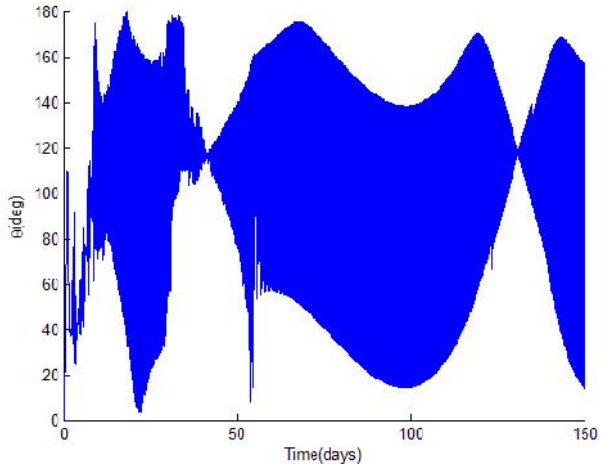

b)

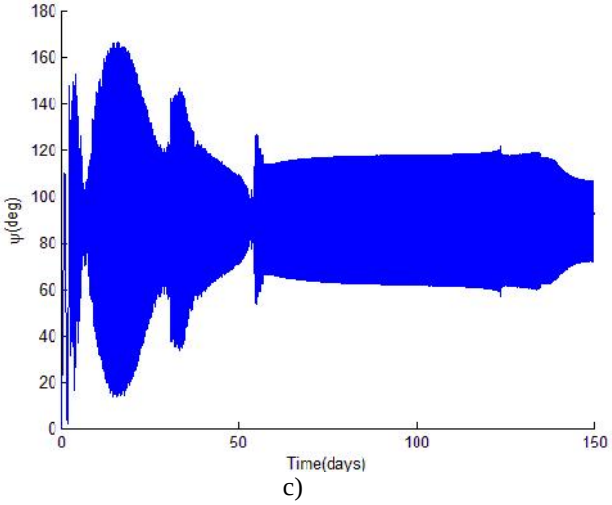

c)

Fig 11 Euler angles of flexible flat plate in 150 days

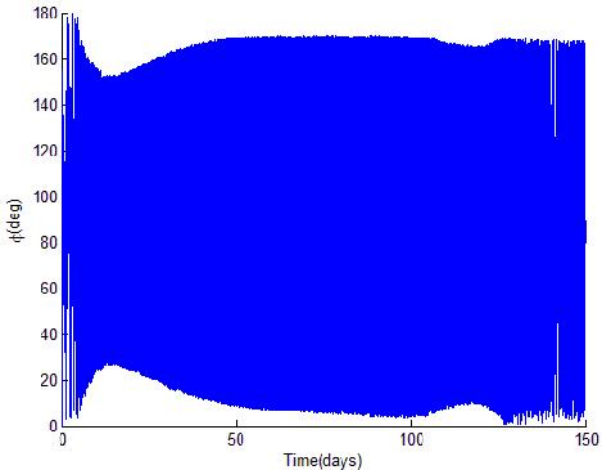

a)

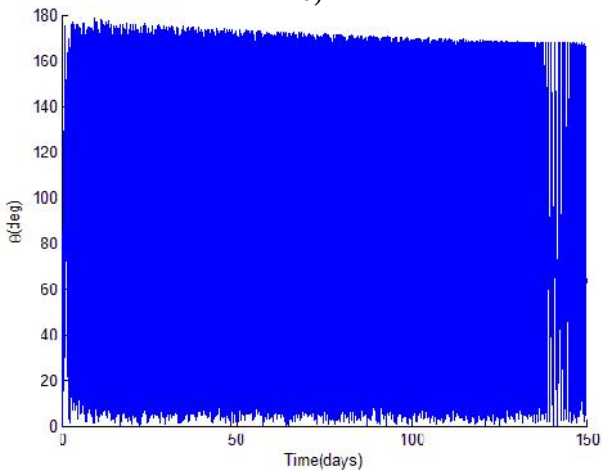

b)

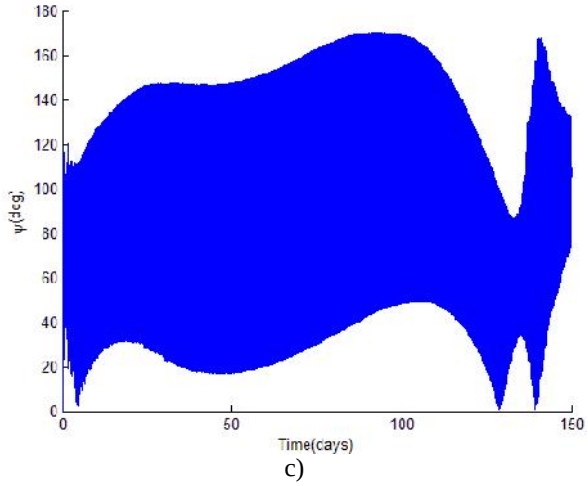

c)

Fig 12 Euler angles of rigid folded flat plate in 150 days

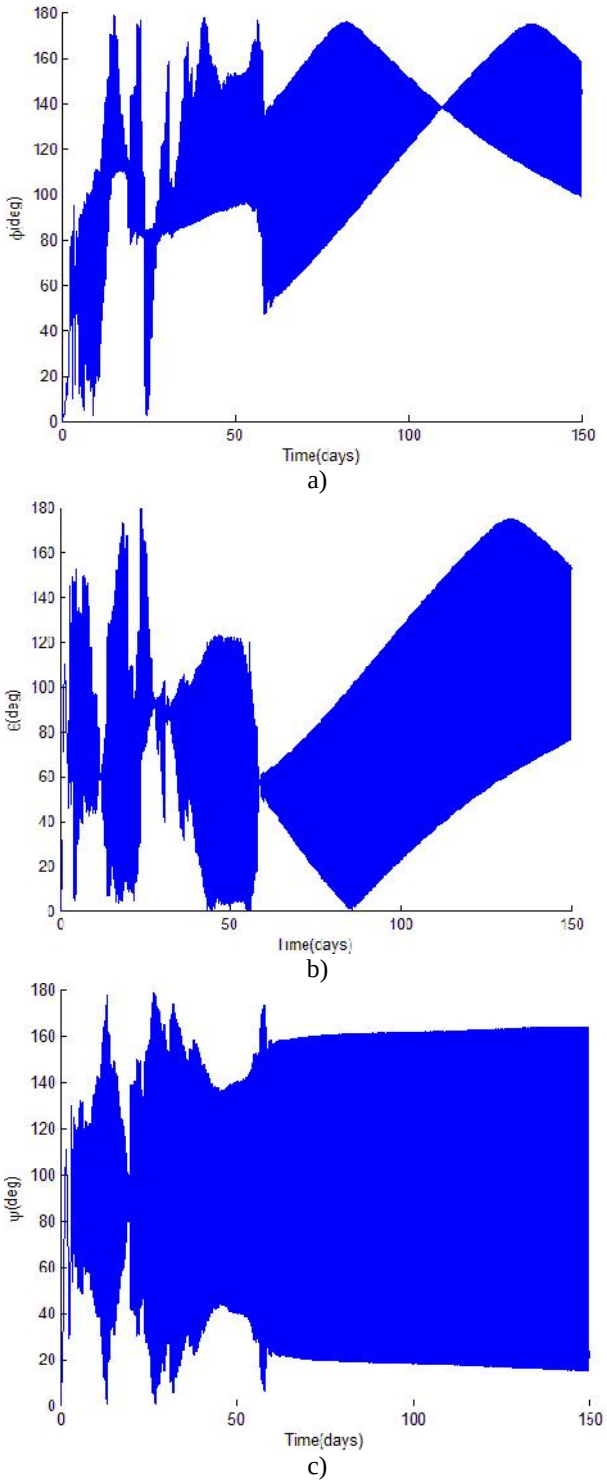

a)

b)

c)

Fig 13 Euler angles of flexible folded flat plate in 150 days

V. CONCLUSION

This paper investigated the attitude and orbital debris of flexible debris in geostationary region in long term period 150 days. The flat plate and folded flat plate have been simulated in rigid and flexible cases by using same properties of PET.

In a propagation of 150 days, some differences can be noticed between the rigid and the flexible cases.. The deformation implies change in the cross-sectional area exposed to the sun, as well as the centre of mass and pressure, and moments of inertia.

From this investigation, when an accurate model of the flexible debris is provided, we can improve to the precision of prediction for the orbit determination , the orbital life time and also investigate the material types of the debris from rotation rates.

Finally, we underline that investigation did not consider large deformations, for which non-linear methods would be required to increase the accuracy of the models for orbital and attitude prediction. In addition, a higher-order propagator shall be used to decrease the simulation time and increase the accuracy in longer periods.

ACKNOWLEDGEMENTS

This work was partly funded by the Air Force Research Laboratory (AFRL) - European Office of Aerospace Research & Development (EOARD).

REFERENCES

1. Desmond, B. *Accessing China's ASAT program*. http://rmit.nautilus.org/forum-reports/0714s-ball/fig3-debris.html 2007.
2. Tariq, M. *Debris From Space Collision Poses Threat to Other Satellites*. 2009.
3. Schildkenecht, T., et al. *Color photometry and light curve observations of space debris in GEO*. in *Proceedings of Advanced Maui Optical and Space Surveillance Technologies Conference*. 2008. Maui Hawaii.
4. Früh, C. and T. Schildkenecht, *Variation of Area-to-Mass-Ratio of HAMR Space Debris objects.* Monthly Notices of the Royal Astronomical Society, 2011. **419**(4): p. 3521-3528.
5. Schildknecht, T., R. Musci, and T. Flohrer, *Properties of the high area-to-mass ratio space debris population at high altitudes.* Advances Space in Research, 2008. **41**(5): p. 1039-1045.
6. Jorgensen, K., et al., *Physical proerties of orbital debris from spectroscopic observation.* Advances in Space Research, 2004. **34**: p. 1021-1025.

7. Mozurkewich, D., *Toward Realistic Dynamics of Rotating Orbital Debris and Implications for Lightcurve Interpretation*, in *Advanced Maui Optical and Space Surveillance Technologies Conference*. 2011: Maui, Hawaii.
8. Dever, J.A., et al., *Mechnical properties degradation of TEFLON FEP returned from the hubble space telescope*, in *36th Aerospace Sciences Meeting&Exhibit*. 1998.
9. Sen, L., et al., *A model to describe the size distribution of satellite breakup debris*, in *63rd International Astronautical Congress*. 2012: Naples, Italy.
10. Murakami, J., et al., *Micro-satellite impact tests to investigate multi-layer insulation fragments*, in *Space Systems Dynamics Laboratory*. 2008, Kyushu University.
11. Liou, J.-C. and J.K. Weaver. *Orbital Dynamics of High Area-To Ratio Debris and Their Distribution in the Geosynchronous Region*. in *Proceedings of the 4th European Conference on Space Debris*. 2005. Darmstadt, Germany.
12. Früh, C. and T. Schildknecht, *Attitude Motion of Space Debris Objects Under Influence of Solar Radiation Pressure And Gravitiy*, in *63rd international Astronautical congress*. 2012: Naples, Italy.
13. Anselmo, L. and C. Pardini, *Long-term dynamical evolution of high area-to-mass ratio debris released into high earth orbits.* Acta Astronautica, 2010. **67**: p. 204-216.
14. Valk, S. and A. Lemaître, *Semi-analytical investigations of high area-to-mass ratio geosynchronous space debris including Earth's shadowing effects.* Advances in Space Research, 2008. **42**.
15. Valk, S., et al., *Global dynamics of high area-to-mass ratios GEO space debris by means of the MEGNO indicator*. Advances Space in Research, 2009. **43**: p. 1509-1526.
16. Flegel, S.K., et al., *Multi-layer insulation model for MASTER-2009.* Acta Astronautica, 2011. **69**.
17. Früh, C., T.M. Kelecy, and M.K. Jah, *Attitude Dynamics Simulation of MLI Space Debris Ojects in Geosynchronous Earth Orbits*, in *AIAA/AAS Astrodynamics Specialist Conference* 2012: Minneapolis MN.
18. Früh, C., T.M. Kelecy, and M.K. Jah, *Coupled Orbit-Attitude Dynamics of High Area-to-Mass Ratio (HAMR) Objects: Influence of Solar Radiation Pressure, Shadow Paths and the Visibility in Light Curves.* Celestial Mechanics and Dynamical Astronomy (CELE), 2013.
19. Vallado, D.A., *Fundamentals of Astrodynamics and Applications*, ed. Third. 2007, New York: Microcosm Press.
20. *Spacecraft radiation torques*, N.A.a.S. Adminstration, Editor. 1969.
21. *Spacecraft gravitational torques*, in *NASA SPACE VEHICLE DESIGN CRITERIA (GUIDANCE AND CONTROL)*. 1969.
22. C.T.F., R., *Advanced applied finite element methods*. 1998, West Sussex: Horwood Publishing Chichester.
23. Rayleigh, L., *Theory of Sound*. second ed. Vol. 2. 1877, New York: Dover.
24. Sheldahl, *The read book*, http://www.sheldahl.com/documents/RedBook%20revised%2020-AUG%20%202012.pdf, Editor. 2012.
25. DesigerData. *PET-Polyethylene terephthalate*. Available from: http://www.designerdata.nl/index.php?material=49&subject=2&pag=8&subpag=1&lang=en.
26. Mott, P.H. and C.M. Roland, *Limits to Poisson's ratio in isotropic materials*, N.R. Laboratory, Editor. 2009: Washington DC.